Summary of the 5th GISMO pool

I. Hermelo, C. Kramer, N. Billot, and S. Leclercq

July 8, 2014

Overview

A total of 297 hours were scheduled at the IRAM 30m radiotelescope for the 5th GISMO pool from April 1st to 11th, 2014. During the four first days of the pool the bad weather conditions did not allow to observe. After that the weather conditions were favorable almost until the end of the pool, allowing to observe a total of 78.5 hours (26.4% of the allocated time). Data for 10 of 12 projects were collected. Depending on the observing strategy, the overheads range from $\sim 10\%$ to $\sim 30\%$. Table 1 summarizes the statistics at the end of the pool.

The median value of the opacities measured during the observations was $\tau_{225\mathrm{GHz}} = 0.296 \pm 0.183$ (see Figure 1). The 37% of the 940 scans collected were taken for projects of the good weather queue (e.g., deep fields, star forming regions with faint extended structures, low-mass prestellar cores), 35% for projects of the bad weather queue (e.g., lensed galaxies, active galactic nucleus, supernova remnants), and the remaining 28% were taken under the "test" project, which was used when unstable weather conditions or technical problems did not allow to observe properly.

For the first time, lateral focus corrections were offered to the observers in both X ($\mathrm{F_x}$) and Y ($\mathrm{F_y}$) directions. The values measured for $\mathrm{F_x}$ and $\mathrm{F_y}$ were always close to 0. During the 5th GISMO pool it was noticed that the FWHM measured with crush improved about $2''$ (from $\sim 18''$ to $\sim 16''$). This improvement is due to changes in the aperture used by crush to measure the FWHM.

A total of 3 healthy scans on Mars were considered to study the flux stability. The median value of the integrated flux density was 561 ± 49 Jy, in good agreement with the value of 581 Jy predicted by the model of E. Lellouch and H. Amri.

GISMO behavior during the 5th pool was good in terms of stability with the exception of some difficulties to resume the observations after the helium recycling due to problems of the GISMO detectors to reach their working temperature. For the first time, in order to avoid known problems of corrupted data, the GISMO crate was restarted daily during the helium recycling routine. The median value of healthy pixels was 98 and the median value of the noise equivalent flux density (NEFD) was

17.9 mJy$\sqrt{\mathrm{s}}$, derived from the Nexus logsheet; i.e., data were reduced using `crush v2.16.b1` and the `default` filtering option. The value of the NEFD is reduced by $\sim 30\%$ when using the `faint` filtering option.

Project			$t_{allocated}$	t_{observed}		t_{real}		t_{target}	
ID	Priority	PI	h	h	%	h	%	h	%
(1)	(2)	(3)	(4)	(5)	(6)	(7)	(8)	(9)	(10)
136-13	5	SS	2.0	2.3	117.4	2.6	132.5	2.31	87.3
156-13	5	PA	30.0	8.4	28.1	9.3	30.9	8.43	90.8
191-13	5	RE	21.0	9.2	44.0	10.4	49.7	9.05	86.8
233-13	5	MAr	26.0	6.1	23.3	7.3	27.9	5.66	77.8
190-13	3	RE	18.0	5.3	29.7	6.0	33.1	5.13	86.2
192-13	3	MAl	27.0	4.0	14.7	4.8	17.7	3.68	76.9
226-13	2	ACT	4.0	1.5	37.0	1.8	43.9	1.44	82.2
227-13	2	MG	39.0	13.3	34.2	15.9	40.8	12.88	81.0
235-13	2	TM	42.0	11.8	28.1	13.6	32.4	11.44	84.1
236-13	2	EW	26.0	0.0	0.0	0.0	0.0	0.00	0.0
242-13	2	AK	52.0	16.9	32.4	21.5	41.4	15.54	72.1
244-13	2	ED	10.0	0.0	0.0	0.0	0.0	0.00	0.0

Table 1: Statistics of the projects scheduled during the 5th GISMO pool. The three first columns correspond to the project name, the rate assigned by the IRAM program committee, and the initials of the PI, respectively. Column 4 is the total amount of allocated hours for each project. Columns 5 and 6 are the total amount of hours that the project was observed and its percentage of completion, respectively. Columns 7 and 8 give the same information than columns 5 and 6 but taking into account the slewing time ($t_{\mathrm{slew}} = 7.6$ min, 34 occurrences) plus the dead time between scans. Finally, columns 9 and 10 correspond to the time spent on the target and the percentage that this time represents in terms of t_{real}.

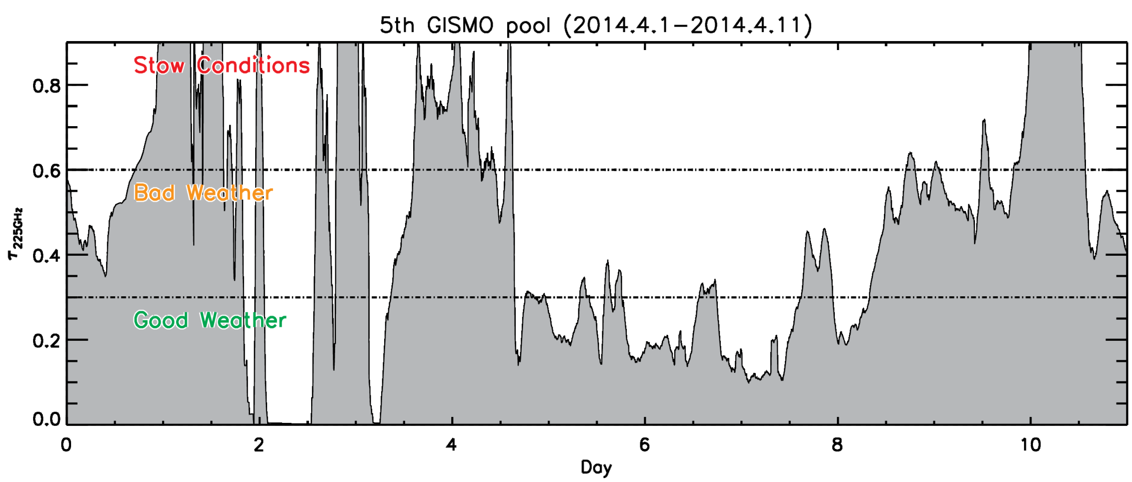

Figure 1: Taumeter readings during the 5th GISMO pool.

1 Pointing

Pointing corrections were systematically done every 60-90 minutes during the 5th GISMO pool. The pointing scans consisted on $1.5' \times 1.5'$ Lissajous maps. The median value and the rms for the pointing corrections in azimuth and elevation are $\Delta\mathrm{Az} = -1.9 \pm 7.7$ and $\Delta\mathrm{El} = -0.9 \pm 7.9$, respectively. Pointing sources were always detected within the array, and in most of the cases the peak is located within the central pixel (see Figure 2). The pointing scans taken during the observations were used to generate a pointing model specific for the 5th GISMO pool[1]. The model gives a blind pointing to $\sim 2''$ rms accuracy in both directions.

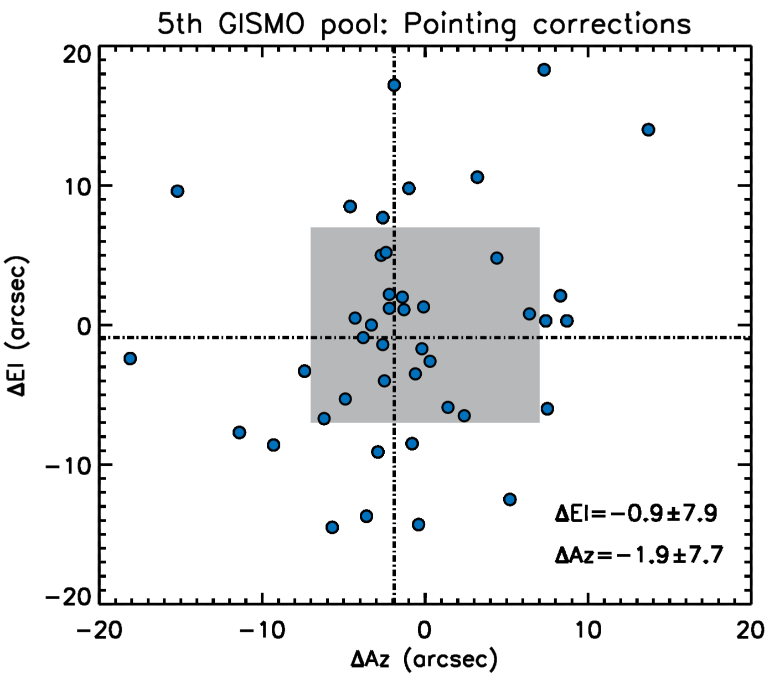

Figure 2: Pointing corrections applied during the GISMO pool. The gray shaded area represents the GISMO pixel size. The black dashed lines correspond to the median values found for ΔAz and ΔEl.

2 Focus

As usual, the focus corrections in the Z direction ($\mathrm{F_z}$) were based on five consecutive $1.5' \times 1.5'$ Lissajous maps taken at five different focus values ($\mathrm{F_z}$, $\mathrm{F_z} \pm 0.6$ mm, $\mathrm{F_z} \pm 1.2$ mm). Focus corrections were calculated with second order fits to the integrated intensity and the FWHM. The new value of the focus was determined as the value that maximizes the flux and minimizes the FWHM (see Hermelo et al. 2013 for details). The median value and the rms of the values used is $\Delta Z = -1.4 \pm 0.8$ mm (see Figure 3).

We want to note that the improvement of about $2''$ (from $\sim 18''$ to $\sim 16''$) in the FWHM noticed during this run has nothing to do with the 30 m but with changes introduced in `crush v2.16.b1` in the aperture used to measure the FWHM.

[1]The new pointing model is included by default in `crush v2.16.b1`.

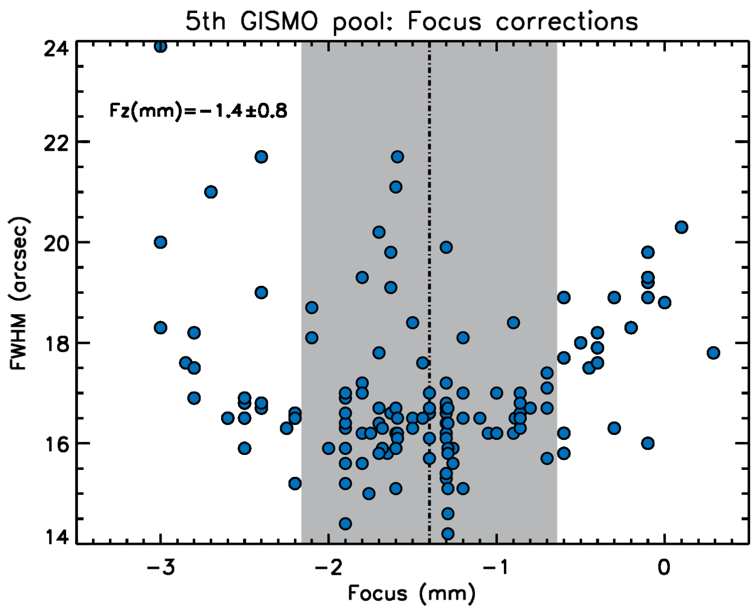

Figure 3: Focus corrections used during the GISMO pool. The vertical black dashed line and the gray shaded area correspond to the median value and to the rms, respectively.

For the first time, lateral focus corrections were offered to the observers in both X (F_x) and Y (F_y) directions. The method to measure the optimal values of F_x and F_y was identical to the method used to optimize F_z with the only exception that the offset between the different values were ± 2 mm and ± 4 mm. The best values found for F_x and F_y were always close to 0 mm. For this reason focus corrections in X and Y were barely used during the pool.

Lateral focus measurements on the point source 3C84 were used to calibrate how the degree of asymmetry of a point source changes when the focus offsets in both X and Y directions change (see Figure 4). The degree of asymmetry of a point source is equal to zero when the telescope is well focused. Therefore, non zero values of the degree of asymmetry indicate that the lateral focus offsets need to be re-calculated (see bottom panel of Figure 5).

3 Calibration

A total of 3 heathy scans taken on Mars during the midnight of April 6th were considered to study the flux stability. The median value of the integrated flux density was 561 ± 49 Jy, in good agreement with the value of 581 Jy predicted by the Mars brightness model of E. Lellouch and H. Amri[2].

We also considered a total of 9 healthy scans taken on Uranus (see Figure 6). The median flux density of these 9 scans is 12.5 Jy and the rms is 0.5 Jy. From this value it is possible to derive a brightness temperature of 91.1 ± 3.6 K, which is $\sim 15\%$ lower than the value of 106.6 K reported by Sayers et al. (2012) using Bolocam data collected between 2003 and 2010.

The measured Mars/Uranus flux ratio, which does not depend on the Jy/counts calibration factor, yielded consistent calibrations in prior runs (within 5% agreement). Therefore, the discrepancy between Mars and Uranus found during the 5th GISMO pool is not related to data reduction. Given

[2]See http://www.lesia.obspm.fr/perso/emmanuel-lellouch/mars/index.php

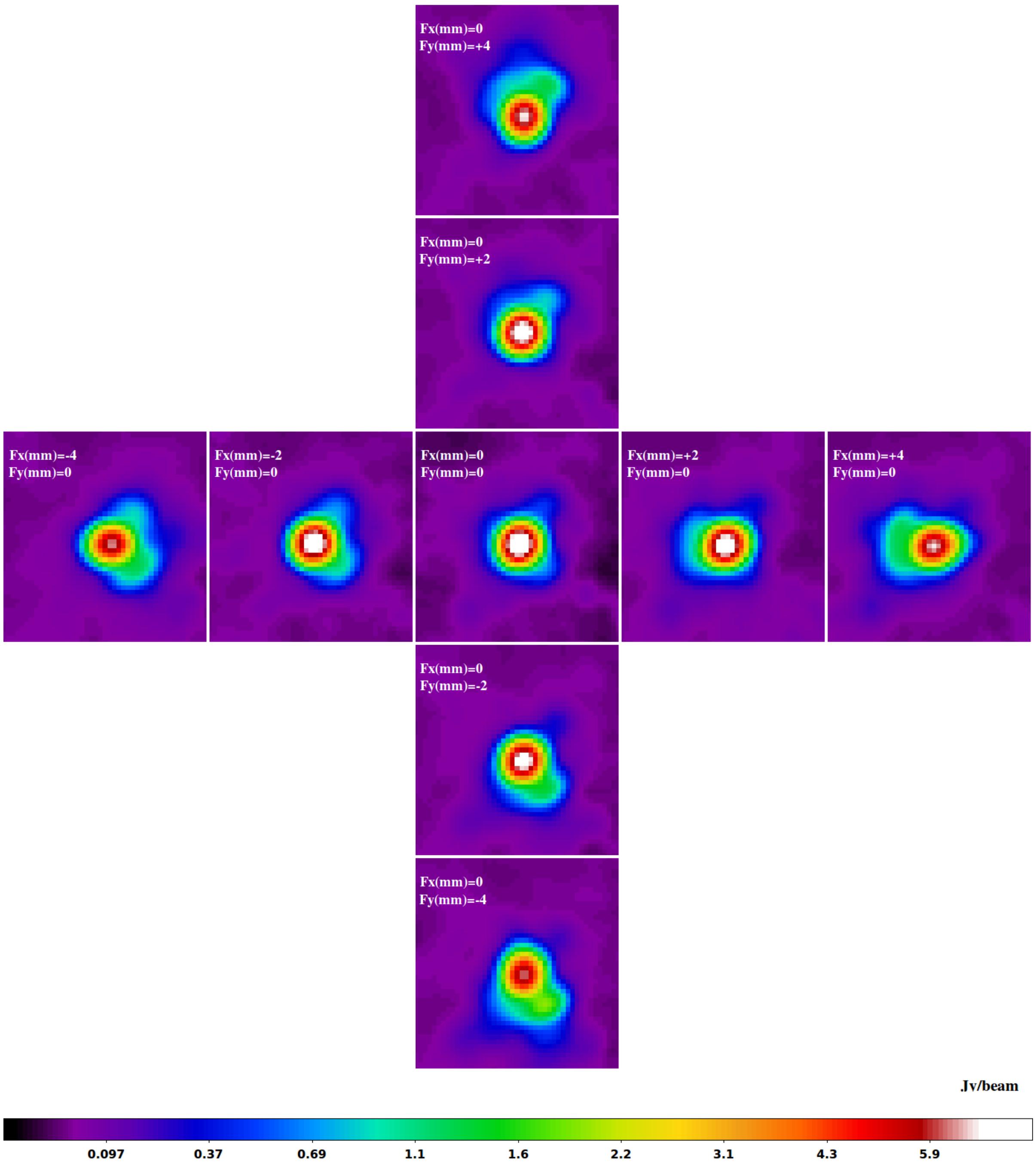

Figure 4: GISMO view of the compact radio source 3C84, the nucleus of the Seyfert galaxy NGC 1275. These maps were used to determine the best values of the lateral focus corrections. Note the response of the peak intensity and the sidelobes to the changes in F_x and F_y. Data were taken on April 4th, 2014 from 13:45 to 14:30 (LT) with F_z fixed to -1.26. The elevation of 3C84 was $\sim 60°$.

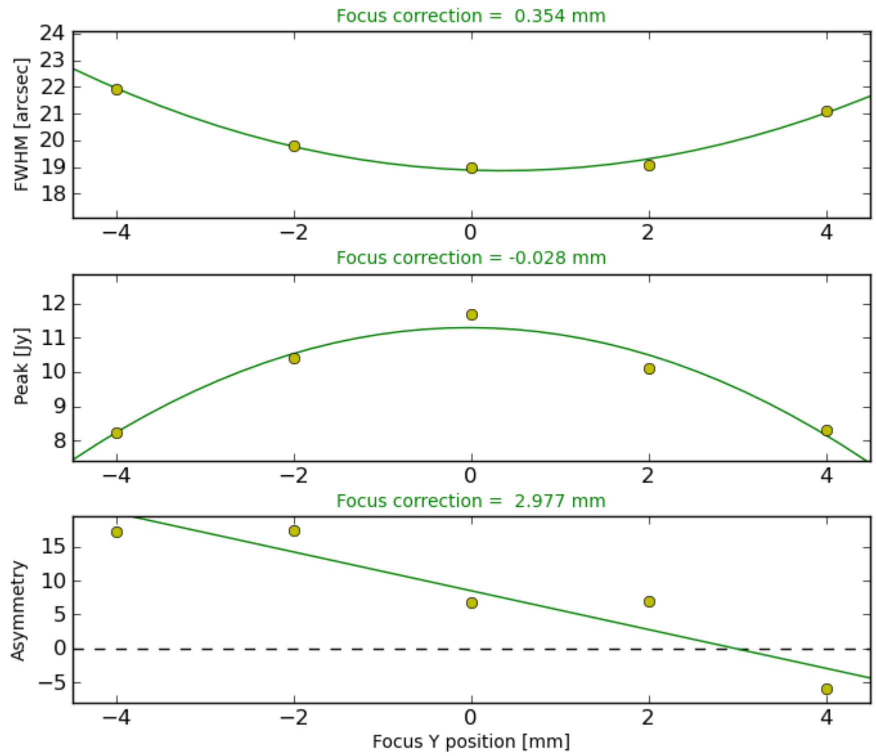

Figure 5: Second order fits to the FWHM and the flux peak (top and middle panel, respectively) were used to derive the optimal focus corrections in both X and Y directions. The quantification of the degree of asymmetry (bottom panel) is still in experimental stage.

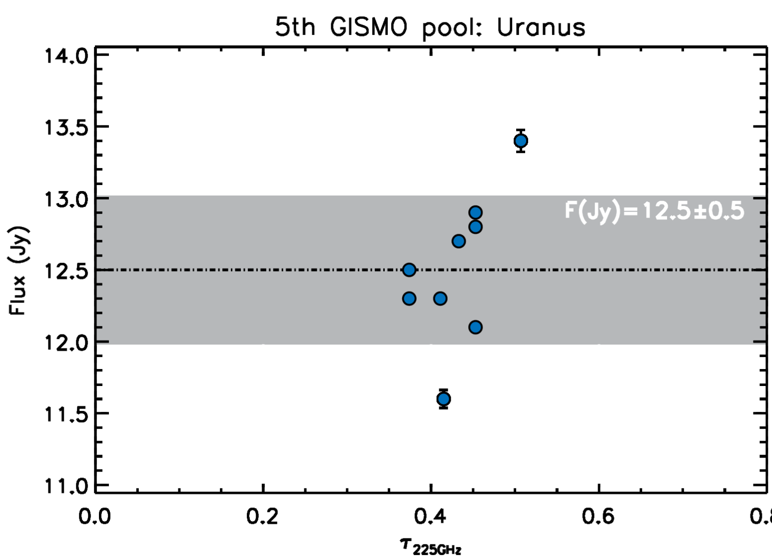

Figure 6: Uranus flux density measurements obtained during the 5th GISMO pool. The horizontal black dashed line and the gray shaded area correspond to the median value and to the rms, respectively.

that Uranus was observed around sunrise, towards the direction of the Sun, there are reasons to suspect that the dish surface was not optimal. Consequently, the usability for calibration purposes of the Uranus scans taken on the 5th GISMO pool might be questionable.

4 Sensitivity

During previous pools (see Hermelo et al. 2013 and Hermelo et al. 2014) it was noticed that the NEFD decreases as the scan speed increases. For this reason the scan speed of the observing modes offered for science scans during the 5th GISMO pool was optimized taken into account the constrains of the telescope control system[3]. Figures 7 and 8 show the trend of the NEFD for scans taken with a scan speed above $60''/s$ (mostly science scans) and scans taken under $60''/s$ (mostly pointing and focus scans for which the scan speed was not optimized).

For the data taken during the 5th GISMO pool we noticed again the anti-correlation between $\tau_{225\,\mathrm{GHz}}$ and the NEFD reported in Hermelo et al. (2014). This trend is appreciable in Figure 8 as a decreasing value of the NEFD for values of $\tau_{225\,\mathrm{GHz}}$ above ~ 0.4. Data statistics were split into scans collected under good ($\tau_{225\,\mathrm{GHz}} \leq 0.3$) and bad weather conditions ($\tau_{225\,\mathrm{GHz}} > 0.3$). As Table 2 shows, the median value of the NEFD is $\sim 18\%$ higher for the scans taken under good weather.

Queue	Number of scans	$\tau_{225\mathrm{GHz}}$	NEFD (mJy $\sqrt{\mathrm{s}}$)	Healthy channels
Bad weather	328	0.489	15.6	98
Good weather	347	0.184	19.0	99

Table 2: Total number of scans collected (column 2), median value of $\tau_{225\,\mathrm{GHz}}$ (column 3), median value of NEFD (column 4), and median value of healthy channels (column 5) for the good and the bad weather queus.

During the 5th GISMO pool it was also noticed that there are "jumps" in the NEFD that might be related with the fridge cycles (see Figures 7 and Figure 9). The origin of these jumps is not well understood but it could be due to He condensation on the array during the refilling. It is well known that He condensation on the array increases noise and that the window is transparent to He, so some of He could penetrate into the dewar at refills. To avoid future problems a new recycling procedure, including a metallic window cover, has been prepared.

References

Hermelo, I., Kramer, C., Billot, N., & González, M. 2013, *Summary of the 3rd GISMO pool*, IRAM 30 m documentation

Hermelo, I., Kramer, C., Billot, N., Lecrercq, S., & González, M. 2014, *Summary of the 4th GISMO pool*, IRAM 30 m documentation

Sayers, J., Czakon, N. G., & Golwala, S. R. 2012, ApJ, 744, 169

[3]The maximum scan speed depends strongly on the elevation and the scanning mode

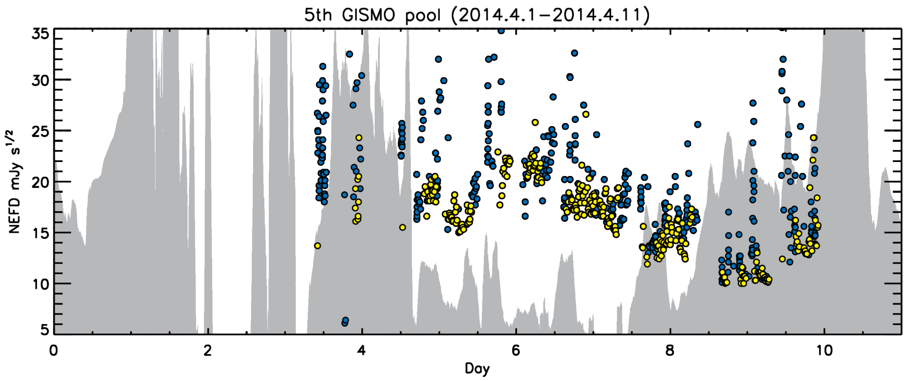

Figure 7: Values of the NEFD mesured during the 5th GISMO *vs* date. Blue filled circles correspond to scanning speeds under $60''/s$ and yellow to scanning speeds above $60''/s$.

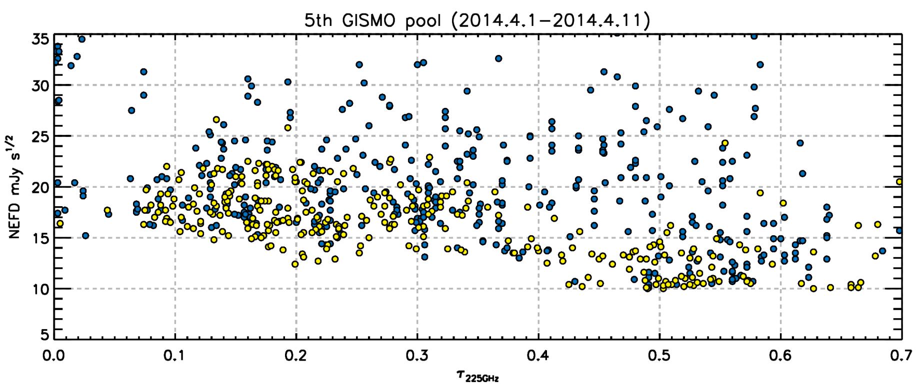

Figure 8: Values of the NEFD mesured during the 5th GISMO *vs* $\tau_{225\,GHz}$. Blue filled circles correspond to scanning speeds under $60''/s$ and yellow to scanning speeds above $60''/s$.

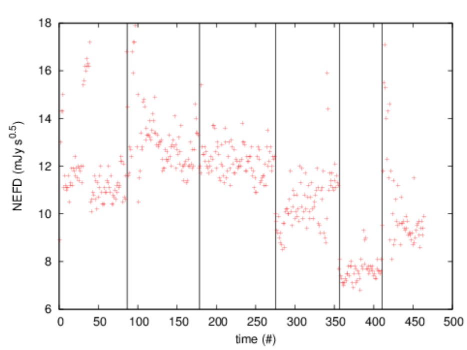

Figure 9: Values of the NEFD mesured during the 5th GISMO *vs* scan number. The vertical lines separate the data from different fridge cycles. Data were reprocessed using the faint filtering scheme. Credits: A. Kovacs